Monitoring of Rotor-Bar Defects in Inverter-Fed Induction Machines at Zero Load and Speed

Thomas M. Wolbank, *Member, IEEE*, Peter Nussbaumer, Hao Chen, *Senior Member, IEEE*, and Peter E. Macheiner

***Abstract*—Rotor-cage fault detection in inverter-fed induction machines is still difficult nowadays as the dynamics introduced by the control or load influence the fault-indicator signals commonly applied. In addition, detection is usually possible only when the machine is operated above a specific load level to generate a significant rotor-current magnitude. This paper proposes a new method of detecting rotor-bar defects at zero load and almost at standstill. The method uses the standard current sensors already present in modern industrial inverters and, hence, is noninvasive. It is thus well suited as a start-up test for drives. By applying an excitation with voltage pulses using the switching of the inverter and then measuring the resulting current slope, a new fault indicator is obtained. As a result, it is possible to clearly identify the fault-induced asymmetry in the machine's transient reactances. Although the transient-flux linkage cannot penetrate the rotor because of the cage, the faulty bar locally influences the zigzag flux, leading to a significant change in the transient reactances. Measurement results show the applicability and sensitivity of the proposed method.**

***Index Terms*—AC motor drives, discrete Fourier transform, fault diagnosis, harmonic analysis, induction-motor protection, monitoring, pulsewidth-modulated inverters, squirrel-cage motors, switching transients, transient response.**

NOMENCLATURE

$\underline{v}_S$	Space vector of the stator voltages in the stator reference frame [in per unit (p.u.)].
$\underline{i}_S$	Space vector of the stator currents in the stator reference frame (in p.u.).
$\underline{\lambda}_R$	Space vector of the rotor-flux linkages in the stator reference frame (p.u.).
r_S	Stator resistance (in p.u.).
l_l	Leakage inductance (fundamental wave) (in p.u.).
$l_{l,t}$	Transient leakage inductance (in p.u.).
$l_{\min}$	Minimum value of transient leakage (in p.u.).
$l_{\max}$	Maximum value of transient leakage (in p.u.).
l_{offset}	Symmetrical part of transient leakage (in p.u.).
l_{mod}	Angle-dependent part of transient leakage (in p.u.).
y_{offset}	Symmetrical part of inverse of transient leakage (in p.u.).
y_{mod}	Angle-dependent part of inverse of transient leakage (in p.u.).
τ	Time (in p.u.).
ω_R	Angular rotor speed (in p.u.).
γ	Angle of asymmetry in stator fixed frame.
δ	Angle between asymmetry and axis of excitation.
θ	Angle of defective rotor bar in the rotor fixed frame.
d	Derivative operator.
Δ	Difference operator.
arg	Argument of complex number.
U, V, W	Machine phase.
α, β	Stator fixed-frame quantities.
Subscripts	
I, II	Index of first, second pulse, and measurement.
$I-II$	Quantity of first pulse minus quantity of second pulse.
$V+, V-$	Quantity when positive or negative pulse is applied to phase V.
Superscripts	
*	Complex conjugate value.

Manuscript received November 3, 2009; revised February 10, 2010, May 12, 2010, and June 21, 2010; accepted July 30, 2010. Date of publication August 19, 2010; date of current version April 13, 2011. This work was supported by the Austrian Science Fund (Fonds zur Förderung der wissenschaftlichen Forschung) under Grant P17595.

T. M. Wolbank and P. Nussbaumer are with the Department of Electrical Drives and Machines, Vienna University of Technology, 1040 Vienna, Austria (e-mail: thomas.wolbank@tuwien.ac.at; peter.nussbaumer@tuwien.ac.at).

H. Chen is with the School of Information and Electrical Engineering, China University of Mining and Technology, Xuzhou 221008, China (e-mail: chenhaocumt@tom.com).

P. E. Macheiner is with Elin EBG Traction, 1140 Vienna, Austria (e-mail: peter.macheiner@tuwien.ac.at).

Digital Object Identifier 10.1109/TIE.2010.2068533

I. INTRODUCTION

IN MODERN industrial drives, dynamic performance is excellent due to field-oriented control methods that can be considered as standard today. The next steps in drive development are going to be driven by attempts to increase reliability and reduce maintenance costs. Although still considered proverbially robust, all components of induction machines are subject to increased stress, particularly when operated in a controlled mode and with repeated load cycles. According to studies, defects in the rotor cage are responsible for about 5% of all breakdowns [1]–[4]. In literature, many attempts have been made to identify rotor defects [5]. The majority of these methods work well if applied to mains-fed machines with stationary load. These main fault indicators are sidebands in the stator current, which are detected using different types of spectrum analysis such as Fourier transform [6], [7], zoom Fourier transform [8], wavelet approaches [9]–[11], pattern-recognition techniques [12], neural networks [13], [14], or Hilbert transform [15]. The load dependence of the sidebands is addressed using genetic algorithm in [16]. A further development to these is proposed in [17] where vibration and external leakage-flux measurement are included. These techniques are all based on stator current-signature analysis (CSA).

Some alternative methods closely related to CSA are the following. The spectra of active and reactive power are the basis for the fault indicator used in [18] for mains-fed and inverter-fed machines [19]. The line-to-neutral voltage spectrum is processed in [20]. Classical CSA and the pendulous oscillation technique are compared in [21]. The envelope of the three-phase currents is employed as fault indicator in [22]. A combination of short-time Fourier transform, wavelet transform, and power-spectral-density techniques is used in [23].

With regard to inverter-operated machines, these techniques are usually limited to steady-state or slowly changing operating conditions of both load and frequency. Fault-induced torque pulsations are detected in [5] by measuring the stator-current spectrum. Wiegner distribution [24] is applied to enable operation at changing stator frequency (10 Hz/sec). In [25] and [26], the phasor of the stator current is processed. In the synchronous frame of reference, the modulus of the phasor is independent of the fundamental-wave supply frequency. Changes introduced by a rotor fault are expressed in the two slip-related sidebands that are then no longer masked by the fundamental wave.

It is also possible to use fundamental-wave models to extract a fault indicator. For example, in [27], a comparison of the torque calculated by the stator equation and the torque calculated by the rotor equation is made, and the data clustered along the rotor angle. The virtual current of a fundamental-wave model is used in [28] to detect rotor defects.

A combination of CSA and a special adaptive algorithm for calculating the magnitude and frequency is used in [29] to eliminate the fundamental wave. The remaining signal is then processed using wavelet analysis. A demodulation technique is applied in [30] to extract the fault-related sideband component in the current spectrum by employing the motor speed obtained from an optical encoder and the stator frequency.

The low-order harmonics $6k \pm 1$ of the pulsewidth modulation (PWM) are identified as producing fault signatures in [31]–[33]. In the case of one fundamental half-wave, a rotor fault introduces even harmonics, which can be used to detect defects.

The pendulous oscillation of the rotor flux is used as a fault indicator in [34]. The slip-dependent modulation of the measured load-current component and its reference value serve as a fault indicator in [35].

Only a few of these methods, however, are also able to deal with the problem of a load torque that is changing with the same frequency as the mechanical angle. For example, this kind of load is usually found when driving compressors.

All of the aforementioned methods require a minimum machine load level in order to detect rotor asymmetries. As the rotor cage is not "operating" in terms of fundamental-wave considerations at zero load, most standard fault indicators fail at this point of operation.

The method presented in [36] is able to detect rotor asymmetry at zero load by identifying the rotor time constant in different spatial directions. However, in order to carry out this identification, the rotor speed has to exceed a configuration-specific minimum level.

In [37] and [38], a pulsating signal is injected in different spatial directions of the machine, and the impedance is calculated. In the case of a broken rotor bar, the impedance is no longer independent of the pulsating-signal direction.

In [39], a rotating voltage phasor is injected with low magnitude to reduce the torque. The harmonic spectrum of the resulting current is analyzed and compared with the healthy machine's spectrum.

The methods presented in [40] are based on rotating injected signals of low magnitude applied to reduce the torque and on pulsating injected signals with changing directions. They observe the angle dependence of the machine parameters in the time domain.

The methods proposed in [41]–[43] are based on an excitation of the machine through special signals such as discrete interval binary sequence and multisine. By analyzing the stator current and the stray flux measured by an external flux sensor, it is possible to detect rotor faults at standstill.

In this paper, a new method is proposed which works at zero load and at zero speed. The difference with the methods applied in [41]–[43] is that no special excitation source or flux sensor is necessary. The method only uses the inverter to establish a voltage pulse excitation and the built-in current sensors to extract the fault indicator. As reported in [44], Cu bars particularly will break over time due to thermal-fatigue cycles, which indicates a slow development of a fault. Therefore, it is not necessary to monitor a drive continuously for that type of fault. The proposed method is also well suited as a start-up test of the drive before commencing normal operation. In standard applications, it is sufficient to carry out such a test every couple of weeks. As the identification is done during startup at zero torque and standstill, oscillations of the load torque as well as dynamic changes of the point of operation due to the dynamics of the current- and/or speed-controller do not influence the obtained fault-indication signal.

The basic idea of the method is to not only limit considerations to the machine's fundamental-wave properties but to also include transient electrical behavior. By applying voltage pulses to the terminals of a machine using the different output states of a voltage-source inverter, transient leakage inductance will dominate the resulting current change. A considerable part of the transient leakage flux is stator-slot leakage and zigzag flux crossing the air gap to bypass the stator-slot openings. In a symmetrical rotor configuration, the cage will prevent the zigzag flux from penetrating the rotor along its whole circumference. With one defective bar, however, there will be a specific change in the transient-flux paths, leading to a measurable asymmetry that is detectable despite operation at no load or even zero flux, as will be shown.

II. Transient Excitation and Asymmetry Detection

The basic principle of the proposed detection method is to identify inherent asymmetries in the machine's transient reactances by comparing the current responses of the three phases to voltage steps.

A simple but very effective way to achieve this is to use the inverter to generate the voltage excitation and the built-in current sensors of the drive for evaluation.

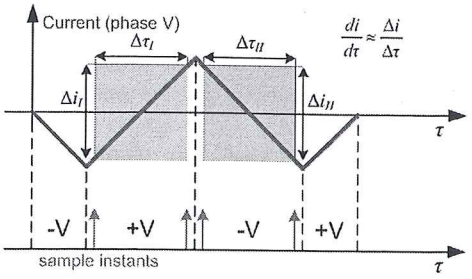

Fig. 1. Symmetrical pulse excitation in one phase axis and sampling of current change.

If a machine is perfectly symmetrical, the well-known stator equation (1) in space phasor representation describes its electrical behavior

$$\underline{v}_S = r_S \cdot \underline{i}_S + l_l \cdot \frac{d\underline{i}_S}{d\tau} + \frac{d\underline{\lambda}_R}{d\tau}. \tag{1}$$

Obviously, the applied voltage phasor $\underline{v}_S$, generated by any of the active switching states of the inverter, leads to a transient current change $d\underline{i}_S/d\tau$. The actual inverter switching state, the dc-link voltage, the value of the leakage inductance l_l, and the stator-resistance voltage drop $r_S \cdot \underline{i}_S$, as well as the time derivative of the rotor flux $\underline{\lambda}_R$ [back electromotive force (EMF)], they all influence this current change.

When applying an active inverter switching state to the terminals of the machine and considering the first transient reaction of the machine current only, there will be two dominant voltage drops: the transient leakage inductance of the machine multiplied by the $d\underline{i}_S/d\tau$ and, if the rotor is magnetized and with the machine running at high speed, the time derivative of the rotor flux (back EMF).

The back EMF, with its magnitude and orientation, will act as a disturbance when identifying the transient reactances.

If two subsequent pulses whose voltage phasors point in opposite spatial directions are applied, the fundamental-wave operating point of the machine is almost unchanged due to the symmetrical nature of the excitation, as can be seen in Fig. 1.

The figure shows a symmetrical pulse sequence consisting of positive and negative switching states of one phase (e.g., −V, +V, −V, +V, at low speed) and the resulting time trace of a corresponding phase current. It is then possible to carry out the measurement (of the resulting current change Δi_I and Δi_{II}), which is symmetrical with respect to the fundamental-wave operating point, using the built-in current sensors of the inverter. The value of the fundamental-wave operating point is indicated by the horizontal time axis in Fig. 1. The switching states are indicated by the dashed lines, and the corresponding voltage phasors (V), the duration ($\Delta\tau$) for taking the current samples, and the resulting current change (Δi) are marked in gray.

The value of the dc-link voltage and the back EMF can be considered constant during the short periods, (some 10 μs) necessary to generate the pulse sequence and perform the measurement. As a result, it is possible to eliminate the influence of back EMF as well as that of the stator resistance using an excitation sequence consisting of two different switching states, as seen in Fig. 1. If the two measurement durations $\Delta\tau_I$ and $\Delta\tau_{II}$ are equal, the elimination is performed simply by taking the difference between the two results Δi_I and Δi_{II}. By combining the phase values of the current changes to one phasor, it is possible to obtain a space phasor of the current difference.

After elimination of the back EMF, the relation between the voltage of the pulse sequence and the measured current change can then be rewritten according to (2). The fundamental-wave operating point is assumed to remain unchanged, which leads to the elimination of the influence of the stator resistance. As the duration of the pulses is only some 10 μs, the change of the back EMF during the measurement can also be disregarded. As a result, the inductance $l_{l,t}$ is the only remaining machine parameter. The value of the fundamental-wave leakage inductance l_l according to (1) differs from the transient leakage inductance responsible for the current change. It is denoted as transient leakage $l_{l,t}$ in the following:

$$\begin{aligned}\underline{v}_{S,I} - \underline{v}_{S,II} &= l_{l,t}\left(\frac{\Delta\underline{i}_{S,I}}{\Delta\tau} - \frac{\Delta\underline{i}_{S,II}}{\Delta\tau}\right) \Rightarrow \underline{v}_{S,I-II} \\ &= l_{l,t}\left(\frac{\Delta\underline{i}_{S,I-II}}{\Delta\tau}\right).\end{aligned} \tag{2}$$

If the machine is perfectly symmetrical as was assumed, the value of $l_{l,t}$ will be a scalar, and the direction of the resulting current slope is parallel to the overall pulse voltage. However, on every real machine, even if faultless, there are always some inherent spatial asymmetries, which also influence the phase values of the transient leakage. As a result, the direction of the applied pulse voltage and current slope will no longer be collinear. In (2), an asymmetry of the machine can be considered by introducing a complex value for the transient leakage $\underline{l}_{l,t}$ that combines the asymmetry of the three phase values in one parameter.

Using a two-axis representation, the magnitude of the transient leakage $|\underline{l}_{l,t}|$ now becomes angle-dependent and can be described by an offset value l_{offset} and an angle-dependent modulation l_{mod}. Assuming only a single dominant asymmetry of the inductance and only taking into account its fundamental wave, the offset and modulation values can be described

$$\begin{aligned}l_{\text{offset}} &= \frac{l_{\max} + l_{\min}}{2} \\ \underline{l}_{\text{mod}} &= \frac{l_{\max} - l_{\min}}{2} \cdot e^{j2\gamma} = l_{\text{mod}} \cdot e^{j2\gamma}.\end{aligned} \tag{3}$$

In (3), $l_{\max}$ and $l_{\min}$ define the maximum and minimum values, respectively, of the transient inductance along the air gap. The angle γ of the modulation gives the spatial position of the maximum inductance within one pole pair. The asymmetry has a period of two with respect to the fundamental wave, which corresponds to the expected modulation of a rotor fault. The influence of a broken rotor bar on the transient leakage is repeated for every pole of the stator winding.

By applying a voltage pulse by the inverter, the overall transient change of the machine current can thus be separated into a "symmetrical" portion determined by l_{offset} and an "asymmetrical" part determined by $\underline{l}_{\text{mod}}$, which leads to an angle-dependent cross coupling in the stator equation, as shown in (4).

Here, the dynamics of the rotor flux $\underline{\lambda}_R$ with respect to the rotor are disregarded due to the rotor time constant that is usually around 10^3 times the time duration considered in the measurements. Its overall time derivative is thus approximated using the term $\omega_R \underline{\lambda}_R$, with ω_R as the rotor speed

$$\underline{v}_S = r_S \cdot \underline{i}_S + l_{\text{offset}} \cdot \frac{d\underline{i}_S}{d\tau} + l_{\text{mod}}\, e^{j2\gamma} \cdot \frac{d\underline{i}_S^*}{d\tau} + j \cdot 2 \cdot \frac{d\gamma}{d\tau} \cdot l_{\text{mod}}\, e^{j2\gamma} \cdot \underline{i}_S^* + j \cdot \omega_R \cdot \underline{\lambda}_R. \quad (4)$$

The complex conjugate of the stator current is denoted as $\underline{i}_S^*$. The goal of the fault-detection method proposed is thus to calculate a fault indicator using the magnitude and angle of $l_{\text{mod}} \cdot e^{j2\gamma}$.

Theoretically, it is possible to calculate this fault indicator directly using (4). However, due to limited sensor accuracy and errors in the machine state variables as well as in the parameters, this direct calculation is not practical.

As already mentioned, the whole measurement cycle takes only a few 10 μs. Thus, it is also possible to eliminate the time derivative of the angle γ in (4), assuming that the rotor position (and thus the position of the defective bar) does not change within that short period. As the magnitude of the asymmetry (defective bar) can be considered constant, its time derivative can therefore also be disregarded.

By applying two subsequent voltage phasors (indexes $_I$ and $_{II}$), it is thus possible to obtain a set of two equations

$$\underline{v}_{S,I} = r_S \cdot \underline{i}_{S,I} + l_{\text{offset}} \cdot \frac{\Delta \underline{i}_{S,I}}{\Delta\tau} + l_{\text{mod}}\, e^{j2\gamma} \cdot \frac{\Delta \underline{i}_{S,I}^*}{\Delta\tau} + j\omega_R \underline{\lambda}_{R,I}$$

$$\underline{v}_{S,II} = r_S \cdot \underline{i}_{S,II} + l_{\text{offset}} \cdot \frac{\Delta \underline{i}_{S,II}}{\Delta\tau} + l_{\text{mod}}\, e^{j2\gamma} \cdot \frac{\Delta \underline{i}_{S,II}^*}{\Delta\tau} + j\omega_R \underline{\lambda}_{R,II}. \quad (5)$$

According to the considerations made, (fundamental-wave current $\underline{i}_{S,I} \approx \underline{i}_{S,II}$ and flux $\underline{\lambda}_{R,I} = \underline{\lambda}_{R,II} = \underline{\lambda}_R$), it is again possible to eliminate the influence of stator resistance and back EMF. By taking the difference between the measurements of the first and the second voltage pulse, (6) is obtained

$$\underline{v}_{S,I-II} = l_{\text{offset}} \cdot \frac{\Delta \underline{i}_{S,I-II}}{\Delta\tau} + l_{\text{mod}}\, e^{j2\gamma} \cdot \frac{\Delta \underline{i}_{S,I-II}^*}{\Delta\tau}. \quad (6)$$

Using (6) to calculate the position γ of the asymmetry implies an exact knowledge of the parameters l_{mod} and l_{offset}, which is not practical for the detection of the fault. In order to reduce the number of mathematical operations as well as the parameter dependence, it is thus advantageous to invert the equations, leading to (7) and finally to (8). In (4)–(7), the complex conjugate is marked with *

$$\frac{\Delta \underline{i}_{S,I-II}}{\Delta\tau} = y_{\text{offset}} \cdot \underline{v}_{S,I-II} + y_{\text{mod}}\, e^{j2\gamma} \cdot \underline{v}_{S,I-II}^* \quad (7)$$

$$\frac{\Delta \underline{i}_{S,I-II}}{\Delta\tau} = \underline{y}_{I-II} \cdot \underline{v}_{S,I-II}. \quad (8)$$

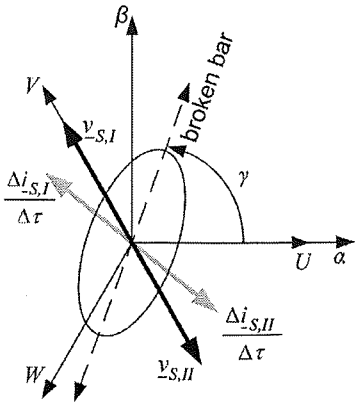

Fig. 2. Transient-current change for pulses in phase direction $V(v_{S,I} = V+, v_{S,II} = V-)$ with assumed asymmetry position $\gamma = 70°$.

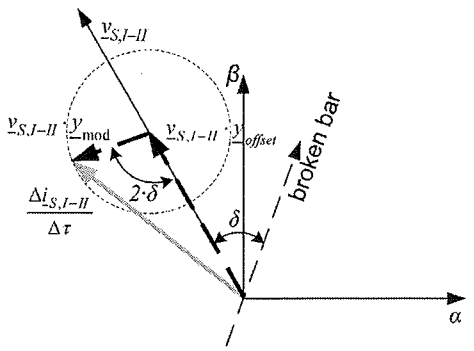

Fig. 3. Resulting transient-current change after signal processing for a given pulse sequence ($v_{S,I} = V+$ and $v_{S,II} = V-$) with assumed asymmetry position $\gamma = 70°$.

The variable $\underline{y}_{I-II}$ contains all the information regarding the asymmetry's magnitude and position

$$\underline{y}_{I-II} = y_{\text{offset}} + \underline{y}_{\text{mod}} = \frac{l_{\text{offset}}}{l_{\text{offset}}^2 - l_{\text{mod}}^2} - \frac{l_{\text{mod}}}{l_{\text{offset}}^2 - l_{\text{mod}}^2} \cdot e^{j\left(2\gamma - 2\arg(\underline{v}_{S,I-II})\right)}. \quad (9)$$

This can be detected, and the position of a possible asymmetry can be tracked by solving (10); a simple calculation for a DSP as the applied pulse sequence is known, and the phasor of the current difference $\Delta \underline{i}_S$ is obtained according to Fig. 1

$$\underline{y}_{I-II} = \frac{\frac{\Delta \underline{i}_{S,I-II}}{\Delta\tau}}{\underline{v}_{S,I-II}}. \quad (10)$$

The minimum number of necessary calculations, which can be performed in real time by every microcontroller, is reached by using a symmetrical excitation in one phase direction (V, see Fig. 1) as shown in Figs. 2 and 3.

As shown in Fig. 2, the two voltage phasors (solid, black) showing the positive and negative axis of phase $V(v_{S,I} = V+, v_{S,II} = V-)$ are applied. The asymmetry of the transient inductance is assumed to have its maximum at $\gamma = 70°$. The asymmetry of the inductance is represented by an ellipse, and

the main axis is denoted by "broken bar." The corresponding phase inductances can be obtained by the intersection of the ellipse with the phase axes. Due to the resulting asymmetry, the measured current changes $\Delta i_{S,I}/\Delta\tau$ and $\Delta i_{S,II}/\Delta\tau$ (gray) are not aligned with the direction of the excitation. (back EMF is disregarded in Fig. 2).

In Fig. 3, the resulting phasor of the current change after signal processing (6) is shown ($\Delta i_{S,I-II}/\Delta\tau$, gray). The resulting difference voltage phasor, ($\underline{v}_{S,I-II}$, thin, black), is pointing in the positive direction of phase V. As each of the voltage pulses has the same magnitude of 1 p.u., (dc-link voltage), the difference voltage phasor results to

$$\underline{v}_{S,I-II} = \underline{v}_{S,V+} - \underline{v}_{S,V-} = 2 \cdot e^{j2\pi/3}. \tag{11}$$

In (3), the inductance is separated into a symmetrical portion denoted as *offset* and an asymmetrical one denoted as *mod*. The symmetrical portion leads to a direction of the resulting current change phasor that is aligned with the direction of the difference voltage phasor. This symmetrical portion of the current change is shown as phasor denoted as $\underline{v}_{S,I-II} \cdot \underline{y}_{\text{offset}}$ (black dashed).

The asymmetrical portion leads to the phasor $\underline{v}_{S,I-II} \cdot \underline{y}_{\text{mod}}$ (black dashed). The asymmetry assumed in the figure is the same as in Fig. 2 and is represented by the phasor denoted as broken bar. The angle $\delta = -50°$ defines the spatial direction of the maximum transient inductance (broken bar) with respect to the direction of the resulting excitation voltage ($\underline{v}_{S,I-II}$) as indicated. This assumed asymmetry leads to an ideal sinusoidal distribution of the inductance with a period that is equal to twice the fundamental wave. If the axis of asymmetry is aligned with the direction of the resulting excitation voltage ($\delta = 0°/180°$), the resulting current change points in the same direction as the applied resulting voltage as if the machine was symmetrical. However, compared with the phasor $\underline{v}_{S,I-II} \cdot y_{\text{offset}}$, its magnitude is either smaller or greater than in the symmetrical case. The value of $\delta = -50°$ shown in the figure thus leads to a resulting (gray) current-change phasor denoted as $\Delta\underline{i}_{S,I-II}/\Delta\tau$. If the angular position of the asymmetry changes, the tip of this resulting current-change phasor moves along the dashed circle as indicated in the figure.

For all practical purposes, it is thus possible to determine the magnitude as well as the spatial position of the asymmetry from the measured trace of the current-change phasor. In order to make the influence of the asymmetry on the transient current slope clear, the magnitude of the asymmetry l_{mod} (circle) has been enlarged in Fig. 3 (compared with the value of l_{offset}). Considering an asymmetry introduced by a broken rotor bar, the modulation will be in the range of a few (5–10) percent.

III. Signal Processing and Measurement Setup

In a practical setup, a processor takes care of the excitation as well as the measurement. The excitation-voltage sequence is well defined in advance. It is thus possible to obtain the values of the difference voltage phasors directly from stored values. For the realization in a processor system, the measurement determines the current difference phasor $\Delta\underline{i}_{S,I-II}/\Delta\tau$ using two current samples of each pulse voltage.

The measured phasor of the current difference contains information on both the value of the symmetrical inductance l_{offset} as well as that of the modulated inductance $\underline{l}_{\text{mod}}$ caused by the asymmetry. The magnitude and angle values of the phasor are thus composed of an offset and a modulation portion that have to be identified separately.

In Figs. 1–3, the signal generation is shown for a resulting difference voltage phasor pointing in phase direction +V.

The value of the symmetrical inductance l_{offset} however is only dependent on the fundamental-wave point of operation. The measurement usually only takes a short time compared with the changes in the fundamental wave. The value of l_{offset} can thus be identified by combining subsequent excitation in different phase directions. If, for example, the excitation includes pulse sequences in the three main phase directions, one resulting phasor can be calculated by adding up the three current-difference phasors. The share of the current difference phasor related to l_{offset} then leads to a zero-sequence component and is eliminated.

The remaining phasor $\underline{v}_{S,I-II} \cdot \underline{y}_{\text{mod}}$ now only contains information on the asymmetry of the machine reactances and is denoted as asymmetry phasor in the following. It will serve as fault indicator in the proposed method.

In order to use the signal for detection of rotor-bar faults, it is necessary to consider and separate all inherent asymmetry components that are present in standard machines.

As even a symmetrical and faultless machine shows some inherent asymmetries, consequently, there are always some modulations detectable in the asymmetry phasor. The reasons for these modulations are spatial saturation, slotting, and rotor anisotropy. These asymmetries superpose on the asymmetry phasor. Identification and separation, however, is possible, as each of the inherent asymmetries show clear deterministic behavior.

The main asymmetry in skewed induction machines is the saturation saliency that is caused by the different levels of saturation arising from the fundamental wave along the circumference. It has a modulation period that is equal to twice that of the fundamental wave (which corresponds to the machine's number of poles). The same modulation period is detectable in the case of a rotor-bar fault as mentioned previously. As the fundamental wave is well known, the identification of the saturation saliency is straightforward. In addition, the magnitude of the saturation saliency depends on the flux and load level of the machine. There is also a dependence of the angular position on saturation with respect to the fundamental-wave current phasor. If necessary, it is possible to identify these dependences in advance. However, as will be shown, it is possible to clearly identify and separate the saturation influence from the fault induced by performing specific measurements.

Another inherent asymmetry results from the openings of the slots in the lamination that cause the slotting modulation, and their number determines the period of this modulation. The point of operation has only negligible influence. If a machine has closed rotor slots, that asymmetry is negligible.

The intermodulation between slotting and saturation asymmetry creates an additional modulation component that also

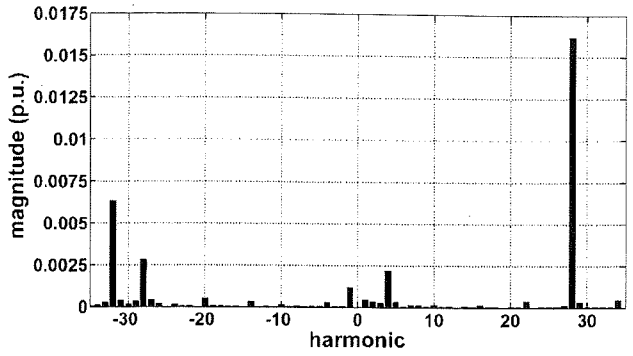

Fig. 4. Harmonic content of the asymmetry phasor of the magnetized faultless induction machine at zero load (horizontal axis: harmonic order scaled to one mechanical revolution).

depends on the point of operation. Its harmonic number is determined by adding the slotting and the saturation harmonic numbers.

The harmonic content of the asymmetry phasor is shown in Fig. 4 for the machine used in this paper. The horizontal axis of the diagram shows the harmonic number where the fundamental wave corresponds to one mechanical revolution of the rotor. It is a two-pole-pair machine with an unskewed rotor and 28 open rotor slots. The machine's point of operation was rated flux level and zero load. As can be seen in the figure, there is a clear, visible, and dominant +28th harmonic together with a small −28th harmonic resulting from the slotting. The +4th harmonic is caused by spatial saturation. The machine has two pole pairs, and thus, the saturation asymmetry results in a second harmonic with respect to the fundamental wave. (Only saturation is detected, not its direction). Thus, the corresponding component is the +4th harmonic shown. In loaded operation, the magnitude of this harmonic will increase considerably, however, always staying below that of the slotting +28th harmonic for unskewed machines.

The −28th harmonic indicates a slight asymmetry in the slotting modulation, and the −32nd harmonic results from the aforementioned intermodulation of saturation and slotting. The spatial difference in the saturation level of the tooth tips is the main reason for this asymmetry.

In Fig. 5, a block diagram of the proposed detection method is shown. First, the voltage pulses are generated by the switching of the inverter. During this pulse sequence, the current is sampled to obtain the current change during a defined period. Then, the phase values of the current changes of different excitation directions are combined to produce a resulting space phasor called an asymmetry phasor. In a separate step, the rotor position of the machine is changed, preferably done using the inverter. The pulse generation and sampling is then repeated until sufficient measurements of different rotor positions are available for a spectral analysis. After applying a Fourier transform, any remaining offset is eliminated. In the final step, the harmonic with the number equaling the pole number of the machine is attained. The magnitude of this harmonic is the fault indicator. As will be shown in the following measurements, the magnitude of this harmonic will experience a very distinct change in case of a broken rotor bar. As already mentioned,

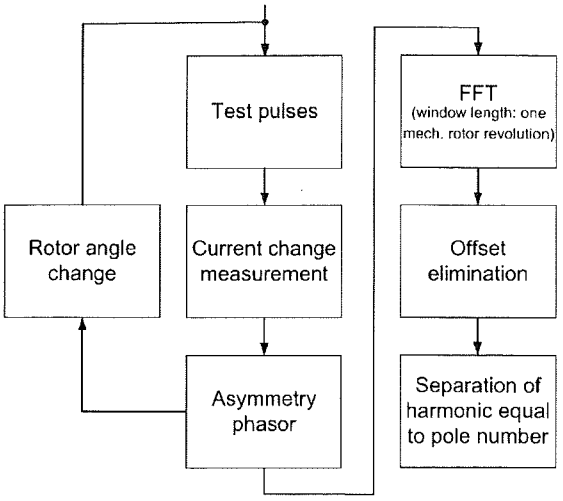

Fig. 5. Block diagram of pulse excitation, measurement, and signal-processing structure.

the asymmetry phasor is also modulated by the slotting of the machine (+28th harmonic). This information can be used to determine how much the rotor has turned if no position or speed sensor is available.

In the case of an inverter structure not allowing repetitive sampling of the current within one PWM period, the whole setup according to Fig. 1 can be extended into subsequent PWM cycles. Then, one whole PWM period is scheduled for each pulse voltage ($\Delta\tau$), and the resulting current change (Δi) during this cycle is obtained as the current difference between two cycles.

IV. Detection of Rotor-Bar Faults Using the Asymmetry Phasor

When voltage pulses are applied to the machine, a transient change in the stator-flux linkage is imposed. In a symmetrical machine, the rotor cage, with its long electrical time constant typically of some hundreds of milliseconds, prevents any transient changes of the rotor flux by blocking the transient flux to the rotor surface.

Stator-slot leakage and zigzag flux, passing the air gap between stator and rotor to bridge the slot openings of both stator and rotor, are thus the dominating transient-flux components. Looking at the harmonic content of the asymmetry phasor (Fig. 4), a strong rotor-slotting harmonic is visible, indicating that there is a considerable portion of the transient flux crossing the air gap to the rotor surface and thus bypassing the stator-slot openings. Measurements on the machines with closed rotor slots only show negligible rotor-slot modulation, which indicates the dominating parameter for this modulation to be the lamination geometry and not the linkage to the loops of the rotor cage. It has to be stressed however that these considerations are limited to the transient flux and differ from fundamental-wave considerations. Simulations of these effects are currently being performed but have not been finished yet, as the calculation of transient magnetic lamination properties including transient hysteresis effects is still very challenging.

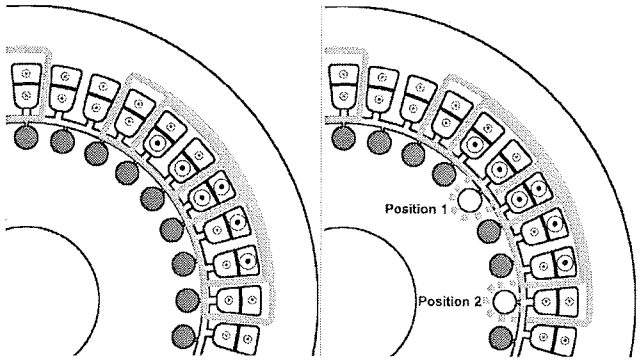

Fig. 6. Spatial distribution of the transient-flux linkage in (left) a faultless machine and (right) machine with (white bars) broken rotor bars on two spatial positions.

In the case of a broken rotor bar, a distinct change in the spatial distribution of the transient-flux linkage can be observed. If one of the rotor bars is broken, the transient zigzag flux can now bypass the rotor-slot opening below the broken bar. This effect is shown in Fig. 6. The left figure shows the spatial distribution of the transient-flux linkage in case of a faultless rotor. Only one pole of the four-pole machine is shown, and an excitation in one single-phase direction is applied. As shown, the transient flux is limited to the air-gap area consisting of stator-slot leakage and zigzag flux. The right figure shows the spatial distribution of a machine with missing rotor bars in two spatial positions. The magnitude of the transient flux bypassing the broken rotor bar at "Position 2" is lower than that bypassing the broken bar at "Position 1." As there is a symmetrical distribution of the machine winding along the air gap, this results in a modulation detectable in the transient flux that correlates with the mechanical angle of the defective bar in the stator-fixed coordinate system. In the case of a machine with two pole pairs, as depicted and used in the measurements, the modulation of the asymmetry phasor has a period equal to four with respect to the mechanical rotor angle, which corresponds to the machine's number of poles.

As mentioned in Section III, the modulation caused by spatial saturation also has a period corresponding to the number of poles. The effect of the broken bar will thus be detectable in the same harmonic order as the saturation harmonic. As the machine considered has four poles, the harmonic to track for the rotor fault detection is the fourth harmonic. A clear separation of the two effects is however possible in different ways.

In one way, the separation is based on the knowledge that the broken rotor bar's fourth harmonic is fixed to the rotor and thus to the mechanical angle, whereas the saturation fourth harmonic is fixed to the stator current phasor and thus to the electrical angle.

A different way of separating the signal components is used in this investigation. It is possible to determine the asymmetry phasor for different angular positions of the defective rotor bar. This leads to separate asymmetry phasors, each at zero load and zero flux level and each for a different angle. As the flux level is zero, the only reason for the fourth harmonic is now the defective rotor bar.

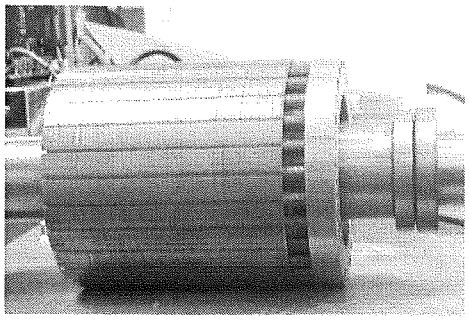

Fig. 7. Rotor with detachable rotor bars. Left ring removed, and the cage and right ring are shifted to the right.

V. Measurement Setup and Results

The measurement setup consists of a machine, a voltage-source inverter, and measurement/control electronics.

The machine has two pole pairs, 36 stator slots, and a specially designed rotor with 28 unskewed bars. In order to enable a nondestructive realization of rotor asymmetries (without drilling holes in the lamination and bars), the rotor cage is built with detachable solid copper bars and two copper end rings. The ends of each bar have one outer and one inner thread, respectively. It is thus possible to insert the bars in the lamination and screw them directly into the end ring that offers the corresponding inner threads. The other end ring has holes drilled to fit the bars exactly. This second ring is fixed by screws to the bars' inner threads. The arrangement is shown in Fig. 7. To make the bars and end ring visible, the cage is shifted to the right.

Unlike a cast rotor cage, this setup allows an individual adjustment of asymmetries without drilling holes in the lamination or end rings. The threads in the bars guarantee good contact with the end rings, also proven by the measurements using the symmetrical cage with all 28 bars inserted.

The measurements were carried out using control electronics programmable under Matlab/Simulink. Pulse excitation and measurement were realized as described in Figs. 1–3 and consisted of a set of two pulses with equal duration pointing in positive and negative directions of one phase. The corresponding sampling of the current was done to determine the current difference phasor $\Delta \underline{i}_{S,I-II}/\Delta\tau$ (using standard industrial current sensors). In order to eliminate the share of the mean value (y_{offset}), the excitation was changed to the three different phase directions. Combining the phasors of all three excitation directions to one resulting phasor eliminates the zero-sequence component as described in Section III. This resulting phasor is denoted as asymmetry phasor in the following.

The first set of measurements was performed on a symmetrical rotor with all bars well fixed in the cage. The machine operating condition was standstill at no load with rated flux level. After injecting the pulse sequences, the asymmetry phasor was calculated; then, the rotor position was changed stepwise using the inverter, and the pulse sequence was injected again to obtain results from one mechanical revolution (see Fig. 5). The best way to show the influence of inherent asymmetries as well as that of a rotor-cage asymmetry is to use spectral

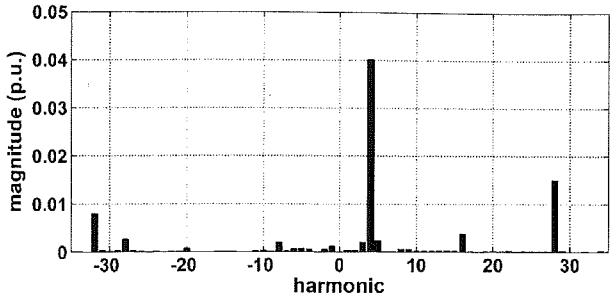

Fig. 8. Harmonic content of the asymmetry phasor of the magnetized machine with one broken bar (horizontal axis: harmonic order scaled to one mechanical revolution; vertical axis: magnitude).

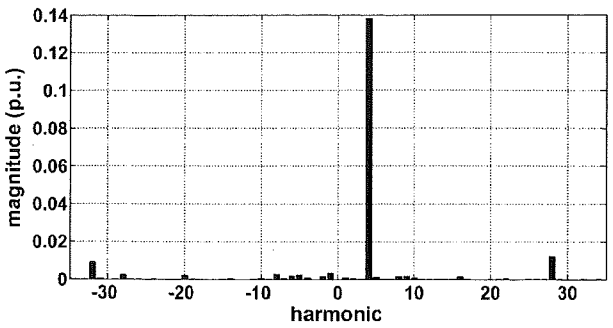

Fig. 9. Harmonic content of the asymmetry phasor of the magnetized machine with two broken bars (horizontal axis: harmonic order scaled to one mechanical revolution; vertical axis: magnitude).

analysis of the asymmetry phasor. It has to be stressed however that the spectral analysis is not the only way to detect bar faults.

As mentioned in Section III, saturation asymmetry will influence the fourth harmonic of the asymmetry phasor with respect to the mechanical period, as the machine has four poles. The harmonic content of the asymmetry phasor for the symmetrical cage is shown in Fig. 4 using Fourier transform. The horizontal axis of the diagram gives the harmonic number where the fundamental wave corresponds to one mechanical revolution of the rotor. The vertical axis has p.u. scaling and represents the magnitude of the harmonic components. The time duration of the excitation is constant throughout the measurements.

The magnitudes obtained with the symmetrical rotor can be identified as $16 \cdot 10^{-3}$ for the +28th (slotting) harmonic, $2,1 \cdot 10^{-3}$ for the +4th (saturation) harmonic, and $6,34 \cdot 10^{-3}$ for the −32nd (intermodulation) harmonic.

Repeating the same measurement with one rotor bar removed reveals the impact of a rotor asymmetry. As can be seen in Fig. 8, the main harmonics except for the +4th remain almost unchanged.

The +28th harmonic (slotting) changes from $16 \cdot 10^{-3}$ to $15 \cdot 10^{-3}$. The −32nd harmonic (intermodulation) changes from $6,3 \cdot 10^{-3}$ to $8 \cdot 10^{-3}$. The biggest change however, as expected, is visible in the +4th harmonic (saturation and broken bar) that rises from $2 \cdot 10^{-3}$ to $40 \cdot 10^{-3}$ by a factor of 20 and now becomes by far the most dominant modulation of the asymmetry phasor. This very distinct change shows how sensitive the proposed fault indicator is.

Repeating the measurement with two broken rotor bars additionally shows the influence of different fault severities. The results are shown in Fig. 9. As can be seen, the harmonics caused by slotting and intermodulation again remain almost unchanged. The increase of the asymmetry, however, has lead to an additional prominent rise of the +4th harmonic from $40 \cdot 10^{-3}$ (one broken bar) to $140 \cdot 10^{-3}$ (two broken bars).

To show the detection sensitivity, a final measurement was performed with one copper rotor bar being replaced by a rotor bar made of steel. Due to the eight times higher resistivity of steel compared with that of copper, a crack in one rotor bar can be imitated. As before, this still results in a significantly increased +4th harmonic of the asymmetry phasor from $2 \cdot 10^{-3}$ to $25,2 \cdot 10^{-3}$ by a factor of 12. In literature, partially broken bars are so far only considered for mains-fed machines.

TABLE I
MAGNITUDE COMPARISON OF THE ASYMMETRY PHASOR'S DOMINATING HARMONICS AT DIFFERENT ROTOR CONDITIONS

Harmonic no.	Symmetric $\cdot 10^{-3}$	steel bar $\cdot 10^{-3}$	1 bar $\cdot 10^{-3}$	2 bars $\cdot 10^{-3}$
-32^{th}	6,3	7	8	9
$+4^{th}$	2,1	25,2	40	140
$+28^{th}$	16	15,4	15	12,3

For practical measurements, holes are usually drilled in the bar/lamination or end ring of the casted cage to simulate a crack. This practice always leads to a combination of broken bar and damaged lamination/end ring.

The proposed method is thus the first by which the detection of only a resistance increase in a single bar without additional lamination/end ring asymmetries is verified on an inverter-fed drive.

Table I summarizes the stated results and lists the magnitude of the asymmetry phasor's dominating harmonics for different rotor conditions. The magnitude of the +4th harmonic varies strongly, whereas the other harmonics remain in the same range. Thus an increase in the magnitude of the asymmetry phasor's +4th harmonic corresponds to an increase in the severity of the rotor defect.

It is however not only possible to detect an asymmetry in the rotor using the asymmetry phasor but also possible to locate the position of the faulty bar on the rotor surface within one pole period by using the angular position of the +4th harmonic with respect to the mechanical rotor angle. Due to this fourth harmonic with respect to the rotor surface, there are, however, four possible positions of the defective bar which lead to the same results. This number four again arises from the pole number of the machine. The following measurement results illustrate this option. Each bar was assigned an index number. A rotor angle of 0° defines the position where the bar with index I is aligned with 0° in the stator fixed reference frame (phase axis U). To determine the position of the bar with respect to the phase axis, a digital camera with a special lens was placed near the air gap. Several measurements were taken, each with a different rotor position to reach one mechanical revolution. The resulting data were processed by a harmonic filter to remove all harmonics except the +4th harmonics. The result is shown in Fig. 10.

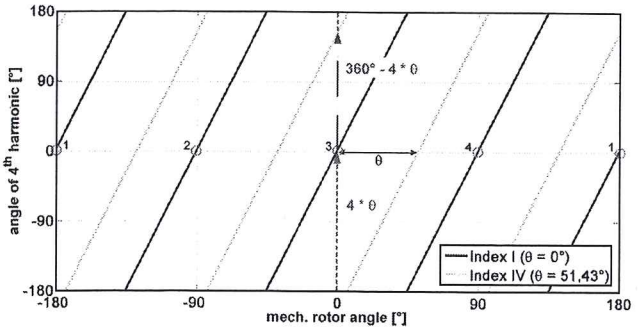

Fig. 10. Angle of the +4th harmonic as a function of the mechanical rotor angle in the case of one broken bar at two different positions (Index no. I and IV). Horizontal axis: mechanical rotor angle; vertical axis: angle of fourth harmonic.

The measurements represent operation without fundamental-wave excitation of the machine at zero-flux level. The horizontal axis of the diagram represents the mechanical angle of the rotor, and the vertical axis shows the angle of the asymmetry phasor's +4th harmonic. Zero degree for the rotor angle means that the position of the rotor bar with index I is aligned with the direction of phase axis U. The solid trace shows the results obtained when the bar with index I is removed. It shows the movement of the fourth-harmonic angle when the rotor is turned by one mechanical revolution. As can be seen, the harmonic angle 0° is obtained for the mechanical positions 0°, ±90°, and 180° (denoted 1..4 in the figure). This trace can also be identified in advance without measurements and can now act as reference for the fault-position detection.

Next, the bar with index I was inserted again, and the bar with index IV was removed. The corresponding results are given by the dashed trace in the figure. The change of the missing bar's position θ can be determined in two ways, as shown.

One way is to take the rotor-angle position where the fourth harmonic angle is equal to zero. This directly delivers the angle θ as shown on the horizontal axis of the figure. The other option is to determine the angle difference of the fourth harmonic with respect to reference trace for one rotor position. This delivers four times the angle θ as shown in the figure.

The machine considered has 28 rotor slots, resulting in an angle difference of $\sim 12,8°$ between two rotor bars. The identified angle difference of $\sim 51°$ between the reference trace and the result for the missing bar with index IV is thus correctly identified.

If machines with pole numbers other than four are used, the harmonic corresponding to the pole number has to serve as fault indicator instead.

VI. Conclusion

This paper has presented a new technique to detect rotor faults in inverter-fed induction machines. It is based on a transient excitation of the machine with voltage pulses applied by the inverter with a duration of some 10 μs. The resulting current change is measured and evaluated and is strongly influenced by the machines' transient slot leakage and zigzag flux. Combining the results obtained from voltage pulses in different spatial positions, an asymmetry phasor is obtained which represents asymmetries in the transient inductance of the machine. A broken rotor bar leads to a distinct change in the distribution of the transient-flux linkage and, thus, to a modulation of the asymmetry phasor when the rotor is turned. This modulation is repeated for every pole of the machine. By identifying the harmonic of the asymmetry phasor that corresponds to pole number of the machine, a bar fault indicator is obtained.

Measurement results on a four-pole 28-rotor-slot machine equipped with a detachable copper rotor cage showed a distinct increase in the fault-indicator magnitude in the case of a broken bar. This increase corresponds to a factor of 20 in the case of one broken bar and a factor of 70 in the case of two broken bars. As proven by measurements, it is possible to identify the position of the broken bar to within one pole using the angle of the fault indicator.

The method presented is noninvasive, as it uses only the current sensors available and is well suited for initial start-up tests of machines as it works at zero speed and load.

Acknowledgment

The authors would like to thank A. Huber from ATB Company for his assistance in constructing the test machine.

References

[1] IEEE Committee Report, "Report of large motor reliability survey of industrial and commercial installation, Part I," *IEEE Trans. Ind. Appl.*, vol. IA-21, no. 4, pp. 853–864, Jul. 1985.

[2] IEEE Committee Report, "Report of large motor reliability survey of industrial and commercial installation, Part II," *IEEE Trans. Ind. Appl.*, vol. IA-21, no. 4, pp. 865–872, Jul. 1985.

[3] P. F. Albrecht, J. C. Appiarius, and D. K. Sharma, "Assessment of the reliability of motors in utility applications—Updated," *IEEE Trans. Energy Convers.*, vol. EC-1, no. 1, pp. 39–46, Mar. 1986.

[4] A. H. Bonnet and C. Yung, "Increased efficiency versus increased reliability," *IEEE Ind. Appl. Mag.*, vol. 14, no. 1, pp. 29–36, Jan./Feb. 2008.

[5] A. Bellini, F. Filippetti, C. Tassoni, and G. Capolino, "Advances in diagnostic techniques for induction machines," *IEEE Trans. Ind. Electron.*, vol. 55, no. 12, pp. 4109–4126, Dec. 2008.

[6] W. Le Roux, R. G. Harley, and T. G. Habetler, "Detecting rotor faults in low power permanent magnet synchronous machines," *IEEE Trans. Power Electron.*, vol. 22, no. 1, pp. 322–328, Jan. 2007.

[7] A. Khezzar, M. Y. Kaikaa, M. E. K. Oumaamar, M. Boucherma, and H. Razik, "On the use of SLot harmonics as a potential indicator of rotor bar breakage in the induction machine," *IEEE Trans. Ind. Electron.*, vol. 56, no. 11, pp. 4592–4605, Nov. 2009.

[8] A. Bellini, A. Yazidi, F. Filippetti, C. Rossi, and G. Capolino, "High frequency resolution techniques for rotor fault detection of induction machines," *IEEE Trans. Ind. Electron.*, vol. 55, no. 2, pp. 4200–4209, Dec. 2008.

[9] S. H. Kia, H. Henao, and G. Capolino, "Diagnosis of broken-bar fault in induction machines using discrete wavelet transform without slip estimation," *IEEE Trans. Ind. Appl.*, vol. 45, no. 4, pp. 1395–1404, Jul./Aug. 2009.

[10] A. Ordaz-Moreno, R. de Jesus Romero-Troncosos, J. A. Vite-Frias, J. R. Rivera-Gillen, and A. Garcia-Perez, "Automatic online diagnosis algorithm for broken-bar detection on induction motors based on discrete wavelet transform for FPGA implementation," *IEEE Trans. Ind. Electron.*, vol. 55, no. 12, pp. 2193–2202, May 2008.

[11] M. Riera-Guasp, J. A. Antonino-Daviu, M. Pineda-Sanchez, R. Puche-Panadero, and J. Perez-Cruz, "A general approach for the transient detection of slip-dependent fault components based on the discrete wavelet transform," *IEEE Trans. Ind. Electron.*, vol. 55, no. 12, pp. 4167–4180, Dec. 2008.

[12] M. Haji and H. A. Toliyat, "Pattern recognition—A technique for induction machines rotor fault detection eccentricity and broken bar fault," in *Conf. Rec. IEEE IAS Annu. Meeting*, 2001, vol. 3, pp. 1572–1578.
[13] B. Ayhan, M.-Y. Chow, and M.-H. Song, "Multiple discriminant analysis and neural-network-based monolith and partition fault-detection schemes for broken rotor bar in induction motors," *IEEE Trans. Ind. Electron.*, vol. 53, no. 4, pp. 1298–1308, Jun. 2006.
[14] F. Filippetti, G. Franceschini, and C. Tassoni, "Neural networks aided online diagnostics of induction motor rotor faults," *IEEE Trans. Ind. Appl.*, vol. 31, no. 4, pp. 892–899, Jul./Aug. 1995.
[15] M. Pineda-Sanchez, M. Riera-Guasp, J. A. Antonino-Daviu, J. Roger-Folch, J. Perez-Cruz, and R. Puche-Panadero, "Instantaneous frequency of the left sideband harmonic during the start-up transient: A new method for diagnosis of broken bars," *IEEE Trans. Ind. Electron.*, vol. 56, no. 11, pp. 4557–4570, Nov. 2009.
[16] H. Razik, M. B. de Rossiter Corrêa, and E. R. C. da Silva, "A novel monitoring of load level and broken bar fault severity applied to squirrel-cage induction motors using a genetic algorithm," *IEEE Trans. Ind. Electron.*, vol. 56, no. 11, pp. 4615–4626, Nov. 2009.
[17] C. Concari, G. Franceschini, and C. Tassoni, "Differential diagnosis based on multivariable monitoring assess induction machines rotor conditions," *IEEE Trans. Ind. Electron.*, vol. 55, no. 12, pp. 4156–4166, Dec. 2008.
[18] G. R. Bossio, C. H. D. Angelo, J. M. Bossio, C. M. Pezzani, and G. O. García, "Separating broken rotor bars and load oscillations on IM fault diagnosis through the instantaneous active and reactive currents," *IEEE Trans. Ind. Electron.*, vol. 56, no. 11, pp. 4571–4580, Nov. 2009.
[19] M. Drif and A. J. Marques Cardoso, "Use of the instantaneous-reactive-power signature analysis for rotor-cage-fault diagnostics in three-phase induction motors," *IEEE Trans. Ind. Electron.*, vol. 56, no. 11, pp. 4606–4614, Nov. 2009.
[20] A. Khezzar, M. E. K. Oumaamar, M. Hadjami, M. Boucherma, and H. Razik, "Induction motor diagnosis using line neutral voltage signatures," *IEEE Trans. Ind. Electron.*, vol. 56, no. 11, pp. 4581–4591, Nov. 2009.
[21] G. Y. Sizov, A. Sayed-Ahmed, C.-C. Yeh, and N. A. O. Demerdash, "Analysis and diagnostics of adjacent and nonadjacent broken-rotor-bar faults in squirrel-cage induction machines," *IEEE Trans. Ind. Electron.*, vol. 56, no. 11, pp. 4627–4641, Nov. 2009.
[22] A. da Silva, R. Povinelli, and N. Demerdash, "Induction machine broken bar and stator short-circuit fault diagnostics based on three-phase stator current envelopes," *IEEE Trans. Ind. Electron.*, vol. 55, no. 3, pp. 1310–1318, Mar. 2008.
[23] J. Cusido, L. Romeral, J. Ortega, J. Rosero, and A. G. Espinosa, "Fault detection in induction machines using power spectral density in wavelet decomposition," *IEEE Trans. Ind. Electron.*, vol. 55, no. 2, pp. 633–643, Feb. 2008.
[24] M. Blödt, D. Bonacci, J. Regnier, M. Chabert, and J. Faucher, "On-line monitoring of mechanical faults in variable-speed induction motor drives using the Wigner distribution," *IEEE Trans. Ind. Electron.*, vol. 55, no. 2, pp. 522–531, Feb. 2008.
[25] S. M. A. Cruz, H. A. Toliyat, and A. J. Marques Cardoso, "DSP implementation of the multiple reference frames theory for the diagnosis of stator faults in a DTC induction motor drive," *IEEE Trans. Energy Convers.*, vol. 20, no. 2, pp. 329–335, Jun. 2005.
[26] S. M. A. Cruz and A. J. Marques Cardoso, "Rotor cage fault diagnosis in three-phase induction motors, by extended Park's vector approach," in *Proc. Int. Conf. Elect. Mach.*, 1998, pp. 1844–1848.
[27] C. Kral, F. Pirker, G. Pascoli, and H. Kapeller, "Robust rotor fault detection by means of the Vienna monitoring method and a parameter tracking technique," *IEEE Trans. Ind. Electron.*, vol. 55, no. 12, pp. 4229–4237, Dec. 2008.
[28] S. M. Cruz, A. Stefani, F. Filippetti, and A. J. Marques Cardoso, "A new model-based technique for the diagnosis of rotor faults in RFOC induction motor drives," *IEEE Trans. Ind. Electron.*, vol. 55, no. 12, pp. 4218–4228, Dec. 2008.
[29] P. S. Barendse and P. Pillay, "The detection of unbalanced faults in inverter-fed induction machines," in *Proc. IEEE Int. SDEMPED*, 2007, pp. 43–51.
[30] A. Stefani, A. Bellini, and F. Filippetti, "Diagnosis of induction machines' rotor faults in time-varying conditions," *IEEE Trans. Ind. Electron.*, vol. 56, no. 11, pp. 4548–4556, Nov. 2009.
[31] B. Akin, U. Orguner, H. Toliyat, and M. Rayner, "Low order PWM inverter harmonics contributions to the inverter-fed induction machine fault diagnosis," *IEEE Trans. Ind. Electron.*, vol. 55, no. 2, pp. 610–619, Feb. 2008.
[32] C. Bruzzese, O. Honorati, E. Santini, and D. Sciunnache, "New rotor fault indicators for squirrel cage induction motors," in *Conf. Rec. IEEE IAS Annu. Meeting*, 2006, pp. 1541–1548.
[33] C. Bruzzese, "Analysis and application of particular current signatures (symptoms) for cage monitoring in nonsinusoidally fed motors with high rejection to drive load, inertia, and frequency variations," *IEEE Trans. Ind. Electron.*, vol. 55, no. 12, pp. 4137–4155, Dec. 2008.
[34] C. Yeh, G. Sizov, A. Sayed-Ahmed, N. Demerdash, R. Povinelli, E. Yaz, and D. Ionel, "A reconfigurable motor for experimental emulation of stator winding interturn and broken bar faults in polyphase induction machines," *IEEE Trans. Energy Convers.*, vol. 12, no. 4, pp. 1005–1014, Dec. 2008.
[35] E. Serna and J. Pacas, "Detection of rotor faults in field oriented controlled induction machines," in *Conf. Rec. IEEE IAS Annu. Meeting*, 2006, vol. 5, pp. 2326–2332.
[36] T. Wolbank, J. Machl, and R. Schneiderbauer, "Detecting rotor faults in inverter-fed induction machines at zero load," in *Proc. Int. EPE-PEMC*, Riga, Latvia, 2004, pp. 1–6.
[37] B. Kim, K. Lee, J. Yang, S. B. Lee, E. Wiedenbrug, and M. Shah, "Automated detection of rotor faults for inverter-fed induction machines under standstill conditions," in *Proc. IEEE Energy Convers. Congr. Expo.*, 2009, pp. 2277–2284.
[38] S. B. Lee, J. Yang, J. Hong, B. Kim, J. Yoo, K. Lee, J. Yun, M. Kim, K. Lee, E. J. Wiedenbrug, and S. Nandi, "A new strategy for condition monitoring of adjustable speed induction machine drive systems," in *Proc. IEEE Int. SDEMPED*, 2009, pp. 1–9.
[39] B. Akin, A. B. Ozturk, H. A. Toliyat, and M. Rayner, "DSP-based sensorless electric motor fault diagnosis tools for electric and hybrid electric vehicle powertrain applications," *IEEE Trans. Veh. Technol.*, vol. 58, no. 6, pp. 2679–2688, Jun. 2009.
[40] C. Concari, G. Franceschini, and C. Tassoni, "Self-commissioning procedures to detect parameters in healthy and faulty induction drives," in *Proc. IEEE Int. SDEMPED*, 2009, pp. 1–6.
[41] C. Demian, A. Mpanda-Mabwe, H. Henao, and G.-A. Capolino, "Detection of induction machines rotor faults at standstill using signals injection," *IEEE Trans. Ind. Appl.*, vol. 40, no. 6, pp. 1550–1559, Nov./Dec. 2004.
[42] A. Mpanda, C. Demian, G. Capolino, and H. Henao, "Detection of induction machines anomalies using stand-still tests," in *Conf. Rec. IEEE IAS Annu. Meeting*, 2003, vol. 3, pp. 1855–1860.
[43] A. Mpanda, C. Demian, and G. Capolino, "Broadband excitation signal techniques for electric machines diagnostics," in *Proc. IEEE Int. SDEMPED*, 2003, pp. 236–241.
[44] M. Hodowanec and W. R. Finley, "Copper versus aluminum—Which construction is best?" *IEEE Ind. Appl. Mag.*, vol. 8, no. 4, pp. 14–25, Jul./Aug. 2002.

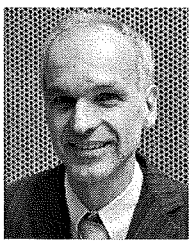

Thomas M. Wolbank (M'92) received the doctoral degree and the Associate Prof. degree from Vienna University of Technology, Vienna, Austria, in 1996 and 2004, respectively.

Currently, he is with the Department of Electrical Drives and Machines, Vienna University of Technology, Vienna, Austria. He has coauthored some 100 papers in refereed journals and international conferences. His research interests include saliency-based sensorless control of ac drives, dynamic properties and condition monitoring of inverter-fed machines, transient electrical behavior of ac machines, and motor drives and their components and controlling them by the use of intelligent control algorithms.

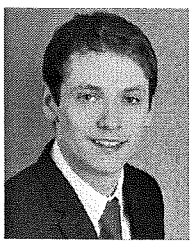

Peter Nussbaumer received the B.Sc. degree in electrical engineering and the M.Sc. degree in power engineering from the Vienna University of Technology, Vienna, Austria, in 2007 and 2009, respectively.

He is currently a Project Assistant with the Department of Electrical Drives and Machines, Vienna University of Technology. His special fields of interest are fault detection and sensorless control of inverter-fed machines.

Hao Chen (SM'08) received the B.S. and Ph.D. degrees from the Department of Automatic Control, Nanjing University of Aeronautics and Astronautics, Nanjing, China, in 1991, and 1996, respectively.

He had been with China University of Mining and Technology, Xuzhou, China, as an Associate Professor in 1998 and has been a Professor since 2001, in the School of Information and Electrical Engineering. He was a visiting Professor at Kyungsung University, Busan, Korea, from 2002 to 2003 and an Adjunct Professor with the University of Western Australia, Perth, Australia, since 2008. He is the author of one book and more than 150 papers.

Peter E. Macheiner received the M.Sc. degree in control engineering from the Vienna University of Technology, Vienna, Austria, in 2005.

From 2005 to March 2009, he was a Project Assistant with the Department of Electrical Drives and Machines, Vienna University of Technology. He is currently a Research and Development Engineer with Elin EBG Traction Company, Vienna, Austria. His special fields of interest are condition monitoring for ac drives as well as control and simulation of electrical machines.